

A Journal of the Gesellschaft Deutscher Chemiker

Angewandte Chemie

GDCh

International Edition

www.angewandte.org

Accepted Article

Title: MnO₂ Electrocatalysts Coordinating Alcohol Oxidation for Ultra-durable Hydrogen and Chemical Productions in Acidic Solutions

Authors: Yan Li, Xinfu Wei, Shuhe Han, Lisong Chen, and Jianlin Shi

This manuscript has been accepted after peer review and appears as an Accepted Article online prior to editing, proofing, and formal publication of the final Version of Record (VoR). This work is currently citable by using the Digital Object Identifier (DOI) given below. The VoR will be published online in Early View as soon as possible and may be different to this Accepted Article as a result of editing. Readers should obtain the VoR from the journal website shown below when it is published to ensure accuracy of information. The authors are responsible for the content of this Accepted Article.

To be cited as: *Angew. Chem. Int. Ed.* 10.1002/anie.202107510

Link to VoR: <https://doi.org/10.1002/anie.202107510>

RESEARCH ARTICLE

MnO₂ Electrocatalysts Coordinating Alcohol Oxidation for Ultra-durable Hydrogen and Chemical Productions in Acidic Solutions

Yan Li,^[a] Xinfu Wei,^[a] Shuhe Han,^[c] Lisong Chen,^{*[a]} Jianlin Shi^{*[b]}

[a] Y. Li, Dr. X. Wei, prof. L. Chen
Shanghai Key Laboratory of Green Chemistry and Chemical Processes
School of Chemistry and Molecular Engineering, East China Normal University
Shanghai 200062, P. R. China
E-mail: lschen@chem.ecnu.edu.cn

[b] Prof. J. Shi
State Key Laboratory of High Performance Ceramics and Superfine Microstructures
Shanghai Institute of Ceramics, Chinese Academy of Sciences
Shanghai 200050, P. R. China
E-mail: jshi@mail.sic.ac.cn

[c] S. H.
Department of Chemistry, Institute of Molecular Plus
School of Science, Tianjin University
Tianjin 300072 (China)

Supporting information for this article is given via a link at the end of the document.

Abstract: Electrocatalytic hydrogen production under acidic conditions is of great importance for industrialization in comparison to that in alkaline media, which, unfortunately, still remains great challenges due to the lack of earth-abundant, cost-effective and highly active anodic electrocatalysts that can be used durably under strongly acidic conditions. Here we report an unexpected finding that manganese oxide, a kind of common non-noble catalysts easily soluble in acidic solutions, can be applied as a highly efficient and extremely durable anodic electrocatalyst for hydrogen production from an acidic aqueous solution of alcohols. Particularly in a glycerol solution, a potential of as low as 1.36 V (vs. RHE) is needed at 10 mA cm⁻², which is 270 mV lower than that of oxygen evolution reaction (OER), to oxidize glycerol into value-added chemicals such as formic acid, without oxygen production. To our surprise, the manganese oxide exhibits extremely high stability for electrocatalytic hydrogen production in coupling with glycerol oxidation for longer than 865 hours compared to shorter than 10 h for OER. Moreover, the effect of the addition of glycerol on the electrochemical durability has been probed via in situ Raman spectroscopic analysis and density functional theory (DFT) calculation. This work opens an unprecedented window that acidity-unstable metal oxide electrocatalysts can be used robustly in acidic media under the presence of certain substances for electrochemical purposes, such as hydrogen production.

Introduction

The rapidly increasing energy demand and environmental pollution have stimulated intensive researches for developing clean, efficient and scalable energy systems. Hydrogen generated from electrochemical water splitting driven by intermittent energy input is of great significance for the renewable energy production, storage and utilization.^[1] This process involves two half reactions of hydrogen evolution reaction (HER) at the cathode and oxygen evolution reaction (OER) at the anode. To date, various cost-effective materials with excellent performance

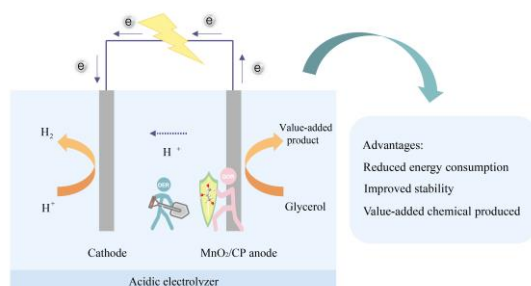
for cathodic HER have been designed for uses in a wide pH range. However, the development of catalysts for anodic OER, which serves as the electron donor for cathodic hydrogen evolution, still remains a great challenge because a high overpotential is necessary for overcoming energy barrier of OER.^[2] Especially, though vitally important for coupling with cathodic HER in the presence of elevated concentrations of proton owing to the much faster kinetics, anodic catalysts in acidic electrolyte have been seldom reported because of either the prohibitive cost of precious metals (e. g. IrO₂ and RuO₂) or the instability of non-noble metals in the acidic and strong oxidative conditions. More notably, the proton exchange membrane (PEM) is currently commercially available and PEM water electrolysis under acidic environment is highly promising in large-scale hydrogen production due to their high current densities, high voltage efficiency, rapid system response and acceptable partial load range.^[3] Therefore, the development of hydrolysis systems as well as corresponding low-cost water splitting electrocatalysts of high activity and stability for acidic electrocatalytic hydrogen production is of great significance and importance, but remains a huge challenge.^[1a, 4] Additionally, anodic OER-produced O₂ is less valuable and the resultant mixture of H₂/O₂ produced by gas crossover during the water decomposition may risk a danger of explosion.^[5]

Alternatively, it is well known that catalysts may exhibit varied activities and stabilities in different anodic reactions. Strategies of small organic molecule oxidation-assisted water splitting for high-efficient H₂ production have emerged most recently, but mostly in alkaline electrolytes, by utilizing low-cost reductive chemical additives (e.g. urea, alcohols and aldehydes) as sacrificial agents to substitute for the kinetic-slow OER, which can greatly lower the cell voltage input and energy consumption, and can even be expected to obtain high value-added oxidation products instead of relative low value-added O₂.^[6] Therefore, non-noble metal electrocatalysts in combination with organic molecule oxidation in acidic electrolyte would be the most appealing and promising for electrocatalytic hydrogen production. However, no reports on electrocatalysts operated in the acidic media by using conventional metal oxides as electrode catalysts can be found to date, due to

RESEARCH ARTICLE

the well-known instability of most transition metal-based materials in the electrocatalytic oxidation of organic compounds in acidic electrolytes.

Thanks to the low cost, earth abundance, low toxicity, rich variation of Mn valence and special Mn-O octahedral field effect, manganese dioxide is a promising electrocatalyst candidate, but usually exhibits considerable compromise between activity and durability and only moderate electrocatalytic performance can be obtained in catalyzing OER in alkaline media, not to mention in acidic electrolytes.^[7] Herein, facile-synthesized manganese oxide catalyst supported on carbon paper (donated as MnO₂/CP) were developed in coordination with alcohol oxidations for the efficient and highly durable hydrogen production in acidic electrolytes (Scheme 1). In this strategy, the oxidation of various alcohols (e.g., glycerol, 1, 2-propanediol and ethylene glycol) were used to substitute for OER, and these alcohols were decomposed into value-added products of carboxylic acid compounds at the anode at a far lower potential than that of OER, along with the promoted H₂ production at the cathode. Especially in the glycerol oxidation reaction, a current density of 10 mA cm⁻² can be achieved at a potential of as low as 1.36 V versus reversible hydrogen electrode (vs. RHE) in acidic aqueous solution, which is 270 mV lower than that of OER. Meanwhile, high value-added liquid product of formic acid, rather than oxygen, can be obtained at the anode to avoid the potential risk of H₂/O₂ explosion in traditional water electrolysis. Impressively and unexpectedly, the electrocatalytic hydrogen production system equipped with MnO₂/CP can be operated for longer than 865 hours under the presence of glycerol, which only lasted for less than 10 hours of OER catalyzed by the same material. The valence state of Mn in MnO₂/CP was slightly increased after glycerol oxidation, but decreased markedly after OER, suggesting that the addition of glycerol can not only reduce the energy input, but also, actually more importantly, prevent the deactivation of the catalyst. The analyses of in situ Raman and DFT calculation demonstrate that the addition of glycerol can enhance the stability of the material via the inhibition of lattice oxygen process and MnO₄⁻ formation.



Scheme 1. Schematic illustration of electrocatalytic H₂ production from acidic aqueous solution of glycerol.

Results and Discussion

Materials characterization

The MnO₂ electrodes were grown in situ on conductive carbon paper (CP) by a facile one-step electrodeposition method.

Scanning electron microscopic (SEM) (Figure 1a and 1b) and transmission electron microscopic (TEM) (Figure 1c) images of the obtained γ -MnO₂ show a nanosheet morphology, which are about ~3.24 nm in thickness as shown in atomic force microscopy (AFM) image (Figure 1d). The side view SEM image and corresponding linear scanning EDX results (Figure S1) reveal a uniform and dense coverage of MnO₂ material on acid-treated CP surface of ~546 nm in thickness. The selected area electron diffraction (SAED) pattern gives a polycrystalline phase structure (Figure 1c, inset), which agrees well with the hereafter results of the X-ray diffraction (XRD). High-resolution TEM (HRTEM) image of MnO₂ further identifies a lattice d-space of 0.248 nm that can be indexed to the (021) lattice planes of γ -MnO₂ (Figure 1e). Additionally, elemental mappings indicate uniform spatial distributions of Mn and O throughout the materials in the view (Figure 1f and Figure S2), and the atomic ratio of manganese to oxygen is 1:1.99, which is consistent with the subsequent X-ray photoelectron spectroscopy (XPS) results.

The crystalline structure of the prepared MnO₂/CP was characterized by XRD. As shown in Figure S3, the diffraction peaks of low intensity except those belonging to graphite (JCPDS no: 411487) from carbon paper can be indexed to (110), (021) and (061) planes of γ -MnO₂ phase.^[8] XPS was employed to further investigate the surface chemical components and valence states of MnO₂/CP (Figure S4). As presented in Figure S4b, the splitting of Mn 3s by the electron exchange interaction upon photoelectron ejection, was used to determine the oxidation state of Mn. The peak energy separation (ΔE) of the splitted Mn 3s in MnO₂/CP is 4.89 eV, which is slightly higher than those literature-reported for MnO₂. According to previous reports, lower valence of manganese will lead to stronger separation of the 3s peaks,^[9] thus, the coexistence of Mn³⁺ and Mn⁴⁺ species in the MnO₂/CP catalyst can be qualitatively concluded, which is consistent with the result of Mn 2p_{2/3} peak fitting result shown in Figure S4c (detailed discussion are given in supporting information). Besides, the high-resolution spectrum of O 1s as shown in Figure S4d can be deconvoluted into three sub-peaks located at 530.03 eV (O1), 531.55 eV (O2) and 533.21 eV (O3), which can be assigned to lattice oxygen, oxygen vacancies and adsorbed oxygen species, respectively.^[10] Meanwhile, the presence of abundant oxygen vacancies, which is usually correlated with the formation of Mn³⁺ species and oxygen evolution activity, has also been evidenced

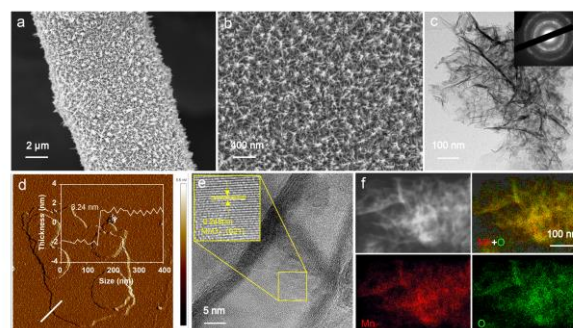


Figure 1. Microscopic analyses of MnO₂/CP catalysts. (a) Low- and (b) high-magnification SEM images of MnO₂/CP. (c) TEM image of MnO₂/CP (the inset shows the SAED pattern). (d) AFM image of MnO₂/CP (the inset shows the corresponding height profile). (e) HRTEM, (f) HAADF-STEM and the corresponding EDS elemental mapping images of MnO₂/CP.

RESEARCH ARTICLE

by electron spin resonance (ESR) measurements as shown in **Figure S5**.

The effects of deposition potential on the composition, microstructure and valance states of the obtained catalysts have been investigated by SEM, XRD (**Figure S6** and **S8**) and XPS measurements (**Figure S7**). As shown in **Figure S7a** and **Table S1**, with the deposition potential increasing from 0.2 to 0.6 V vs. SCE, the peak energy separation ΔE of the splitted Mn 3s decreases from 5.35 eV to 4.89 eV, then remains almost unchanged at further increased deposition potential from 0.6 to 1.0 V vs. SCE, suggesting a relatively lower ratio of Mn^{3+} to Mn^{4+} of the catalysts synthesized at the potentials higher than or equal to 0.6 V vs. SCE, which is also supported by the energy level measurements of Mn 2p_{2/3} (**Figure S7b** and **Table S2**). Moreover, all these results correspond well with the XRD results, that is, the characteristic peak of γ -MnO₂ can only be observed in the manganese oxide catalysts deposited at higher than or equal to 0.6 V (**Figure S8**). Additionally, the XPS O1s spectra imply enhanced density of oxygen vacancies in the catalysts at lowered deposition potential (**Figure S7c** and **Table S2**), which corresponds to the elevated ratio of Mn^{3+} to Mn^{4+} and the negative effect of lowering deposition potential on the formation of γ -MnO₂.

Electrochemical behavior

The electrocatalytic performance of MnO₂/CP towards various alcohols (glycerol, ethanol, ethylene glycol (EG), 1, 2-propanediol (1, 2-P), 1, 3-propanediol (1, 3-P) and 1-propanol (1-P)) oxidations was evaluated in 0.005 mol/L (donated as M) H₂SO₄ at a scan rates of 2 mV s⁻¹ using a typical three-electrode configuration. As displayed in **Figure 2a**, all the current densities obtained in various kinds of acidic aqueous solutions of alcohols are markedly higher than that in alcohol-free electrolyte, among which the glycerol-containing solution gives the highest current density. According to these preliminary electrochemical characterizations, glycerol was selected as the representative candidate for further detailed studies. **Figure S9** shows the liner sweep voltammetry (LSV) curves obtained in 0.005 M H₂SO₄ containing varied concentrations of glycerol catalyzed by the MnO₂/CP. Apparently, MnO₂/CP exhibits a relatively low current density in the absence of glycerol, indicating a rather low OER activity, whilst the current density increases along with the increase of glycerol concentration and reaches the maximum at 0.2 M glycerol. Note that at the increased concentration of glycerol above 0.30 M, the current density decreases probably due to the poor conductivity of the mixed solution.^[11] In order to further verify the electrochemical activity of MnO₂/CP, the LSV curves in the absence and presence of 0.2 M glycerol were recorded subject to the correction by iR compensation with respect to the solution resistance as shown in **Figure 2b**. A current density of 10 mA cm⁻² can be achieved at an applied anodic potential of 1.36 V (vs. RHE) for glycerol oxidation reaction (GOR), which is remarkably 270 mV lower than that for OER (1.63 V vs. RHE). Moreover, the potential reductions for glycerol oxidation are at least 310 mV and above to reach the current densities of 20, 40, 60 and 80 mA cm⁻², implying more favorable alcohol oxidation compared to OER at elevated current densities (**Figure 2c**). Such anode potential reductions are indeed appealing under acidic conditions in comparison with previous literature reports even on precious metal catalysts^[4c, 4d, 12] (**Figure S10**). Moreover, the corresponding Tafel slope of GOR is 242.1 mV dec⁻¹, which is also much lower than that of OER (352.6 mV dec⁻¹), demonstrating a more favorable electrocatalytic kinetics of GOR than that of OER

(**Figure 2d**). For comparison, manganese oxide synthesized by cyclic voltammetric cycles supported on CP (denoted as MnO₂/CP-CV) has also been evaluated under the same condition (**Figure S11**). As shown in **Figure S12**, MnO₂/CP shows a lower onset potential than that of MnO₂/CP-CV for GOR, indicating the higher electrochemical GOR performance of the former. The electrochemical impedance spectra (EIS) show a relatively lower impedance of MnO₂/CP, indicating the faster charge transfer on the electrode surface (**Figure S13a**) than others. Furthermore, the results of the double-layer capacitances (C_{dl}) calculated from the cyclic voltammetry curves point to a smaller C_{dl} value of MnO₂/CP-CV (0.762 F cm⁻²) than that of MnO₂/CP (0.909 F cm⁻²), demonstrating a significantly larger electrochemical surface area (ECSA) and denser exposed active sites of the catalyst MnO₂/CP synthesized by potentiostatic technique (**Figure S13b-d**).

To obtain the optimal GOR performance, the synthetic parameters, such as the deposition time period, deposition potential and the pretreatment of the carbon paper have been modulated. Firstly, the electrocatalytic performances of manganese oxides synthesized at varied deposition durations (detailed information shown in **Table S3**) have been tested under the same condition and the results are shown in **Figure S14-15**. Apparently, the thicker-deposited MnO₂ catalysts show higher electrocatalytic activities than the thinner ones, as demonstrated by the enhanced current densities at increased material loadings. However, it should be noted that the 8.98 C cm⁻² is the optimal catalyst loading beyond which the activity of the catalyst reaches a plateau, which can be attributed to the intrinsically limited proton-electron transport and transfer rates in catalysts.^[13] In addition, the importance of carbon paper pretreatment for the deposition of manganese oxides should be emphasized. As evidenced in **Table S4**, the XPS results of the Acid-CP show the increased oxygen amount on the surface of carbon paper after acid treatment. When using the untreated CP (donated as UCP) as substrate, the obtained MnO₂/UCP shows a much lower amount of charge passing-through (4.33 C cm⁻²) during the electrodeposition than MnO₂/CP (8.98 C cm⁻²), indicating an inferior catalytic oxidation activity of glycerol and the important role of the oxygen-containing groups on the CP surface for anchoring the catalytic materials (**Figure S16** and **Table S3**).^[14] Furthermore, a series of manganese oxide catalysts prepared at varied deposition potentials have been investigated for GOR (**Figure S17**). 0.6 V (vs. SCE) has been selected as the optimal potential for catalyst fabrication in terms of the catalytic activity and energy consumption.

RESEARCH ARTICLE

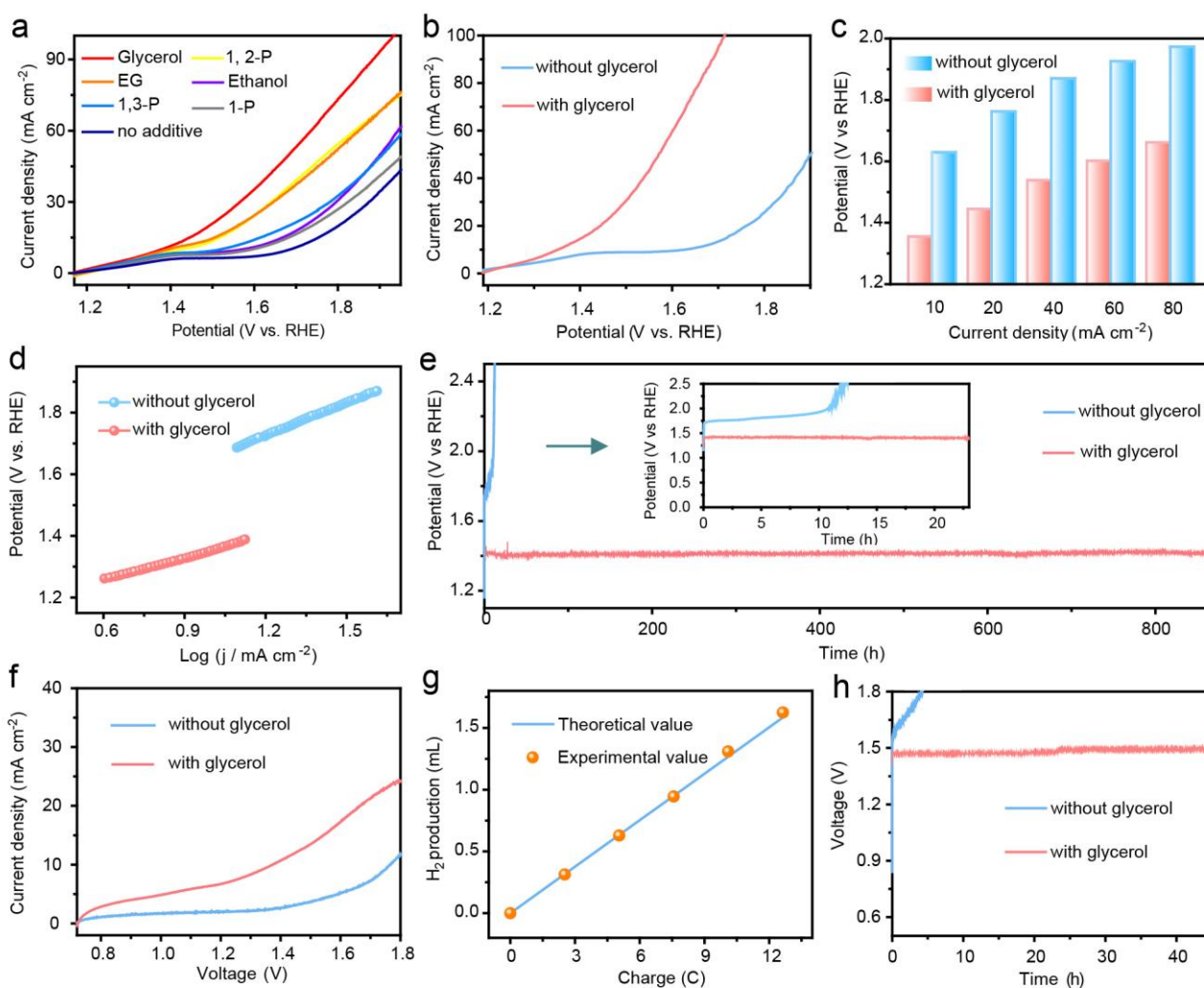


Figure 2 Electrochemical performances of the manganese oxide catalysts. (a) Polarization curves of MnO_2/CP anode in the absence and presence of various kinds of alcohols under acidic conditions at the scan rate of 2 mV s^{-1} . (b) iR-corrected polarization curves of MnO_2/CP anode in $0.005 \text{ M H}_2\text{SO}_4$ with and without the addition of 0.2 M glycerol at the scan rate of 2 mV s^{-1} . (c) Anodic potential comparison of MnO_2/CP at varied current densities ($10, 20, 40, 60$ and 80 mA cm^{-2}) in $0.005 \text{ M H}_2\text{SO}_4$ with and without the addition of 0.2 M glycerol. (d) Tafel plots for glycerol oxidation and OER derived from the LSV results. (e) Chronopotentiometric curves of MnO_2/CP for glycerol oxidation and OER at a constant current density of 10 mA cm^{-2} . (f) Polarization curves over a $\text{MnO}_2/\text{CP} \parallel \text{Pt/C/CP}$ electrolyzer with and without the addition of 0.2 M glycerol addition. (g) Comparison between GC-measured and theoretically calculated H_2 quantities. (h) Time dependences of the electrolyzer voltage over a $\text{MnO}_2/\text{CP} \parallel \text{Pt/C/CP}$ cell with and without the addition of 0.2 M glycerol at 10 mA cm^{-2} .

It is well known that the long-term stability of anodic catalysts under acidic conditions is a great challenge for electrocatalytic water splitting, especially for non-precious metal electrocatalysts. Therefore, the durability of MnO_2/CP electrode for glycerol oxidation and OER has been evaluated in low pH solutions with and without glycerol addition by prolonged chronopotentiometric assays at a constant current density of 10 mA cm^{-2} . According to the experimental results in **Figure 2e**, the high activity of the MnO_2/CP can be maintained for longer than 865 hours (still under test) at a low potential of approximately 1.40 V vs RHE without activity significant decay in $0.005 \text{ M H}_2\text{SO}_4$ solution with the addition of 0.2 M glycerol. Long-term glycerol oxidation has also been confirmed in stronger-acidic 0.05 M and $0.5 \text{ M H}_2\text{SO}_4$ solutions containing glycerol (**Figure S18**). Furthermore, the MnO_2/CP electrode also shows long-time stability at a much elevated current density of 60 mA cm^{-2} (**Figure S19**). On the contrary, the OER potential output can be maintained relatively stable for only 10 and 1 h before soaring in the absence of glycerol

at 10 and 60 mA cm^{-2} , respectively. Moreover, MnO_2/CP also shows remarkably higher stability in various alcohol-containing electrolytes than that of OER in the absence of alcohol additions (**Figure S20**). These results suggest that the coordinative combination between manganese oxide catalyst and alcohol oxidation can not only decrease the potential needed, but also unexpectedly and extremely durably electro-oxidize alcohol, especially glycerol, in strongly acidic media for the concurrent electrochemical productions of hydrogen and value-added chemicals.

In order to highlight the excellent performance of the $\gamma\text{-MnO}_2$ electrode, other manganese dioxides of different crystalline phases ($\alpha\text{-}$, $\beta\text{-}$, $\delta\text{-}$, $\epsilon\text{-}$ and $\lambda\text{-MnO}_2$) were also prepared (See details in the supporting information) according to previously reported methods^[15] and characterized, and their performances of glycerol electro-oxidation were tested. As shown in **Figure S21**,

RESEARCH ARTICLE

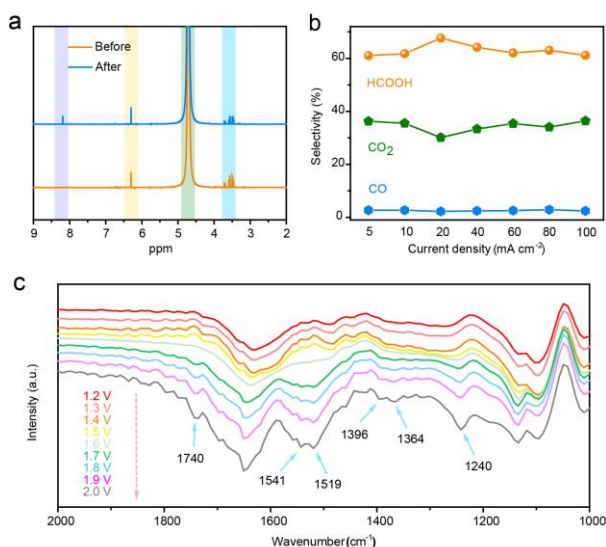


Figure 3 Product analyses for glycerol oxidation. (a) ¹H NMR spectra of electrolyte before and after long-term anodic electrochemical test. Maleic acid was added as an internal standard. Color codes: Formic acid (purple), glycerol (blue), Maleic acid (yellow) and H₂O (green). (b) Selectivities for formic acid, CO₂ and CO production at varied current densities. (c) In situ electrochemical FTIR spectra of MnO₂/CP at different potentials in an acidic glycerol solution.

the XRD patterns can be indexed to α -MnO₂ (JCPDS 44-0141), β -MnO₂ (JCPDS 24-0735), δ -MnO₂ (JCPDS 80-1098), ϵ -MnO₂ (JCPDS 30-0820) and λ -MnO₂ (JCPDS 44-0992) from top to bottom, respectively. SEM images of these manganese dioxides are displayed in **Figure S22**. The LSV curves for GOR catalyzed by the different manganese dioxides show the highest activity of γ -MnO₂. Furthermore, the stability of these manganese oxide samples for glycerol oxidation were tested in acidic solutions by chronopotentiometric assays at 10 mA cm⁻². The higher activity of the γ -MnO₂/CP can be maintained at the lower potential than other catalysts, indicating the great potential of the γ -MnO₂/CP in this system.

With the excellent electrocatalytic performance of MnO₂/CP for the anodic GOR in hand, a two-electrode electrolyzer using MnO₂/CP as the anode and commercial Pt/C/CP as the cathode has been assembled using a glycerol-added, acidic aqueous electrolyte. As a contrast, conventional overall water electrolysis was examined using the same system without any chemical additive. As observed in **Figure 2f**, the electrolyzer in the presence of glycerol requires a cell voltage of as low as 1.38 V to reach the current density of 10 mA cm⁻², leading to much lowered energy input compared with that at the voltage up to 1.78 V required in acidic aqueous solution without adding glycerol. Additionally, the H₂ amount generated at the cathode matches well with the theoretical values, suggesting a Faraday efficiency (FE) up to 100% (**Figure 2g**). Most importantly, the ultra-high durability of MnO₂/CP in acidic electrolyte with glycerol is further verified by the sustained chronopotentiometry measurements, where the operation voltage of 1.47 V can be maintained for over 45 h without significant increase. However, a rapid rise of voltage is inevitable in pure water splitting in as short as 4 h, in accordance with the general knowledge of poor stability of MnO₂ in acidic media without the addition of glycerol (**Figure 2h**).

Based on the high activities and stabilities of MnO₂/CP in electrocatalytic hydrogen production system, the compositions of the anodic reaction products after the addition of glycerol were first analyzed by NMR after long time chronopotentiometry at the constant current density of 10 mA cm⁻² in 0.2 M glycerol aqueous solution. As evidenced in **Figure 3a** and **Figure S23a-23c**, formic acid, as the liquid product of glycerol oxidation, can be detected by ¹H and ¹³C NMR spectroscopy, featuring an average but highly stable Faradaic efficiency (FE) of ~53% in the long period (96 hours) electrocatalytic glycerol oxidation process (**Figure S23c**), which proves the excellent stability of the MnO₂/CP electrode for the generation of formic acid by glycerol oxidation under the experimental conditions. Products obtained by chronopotentiometry at varied current densities have also been tested. The resultant FE and the selectivity towards formic acid production are 47%~56% (**Figure S23d**) and 61%~68% (**Figure 3b**), respectively. Moreover, the gas products, namely CO₂ and CO, have also been produced according to the gas chromatographic results, and their FEs and selectivity have been calculated as presented in **Figure 3b** and **Figure S23d**. Moreover, no oxygen can be detected at the anode electrode in the whole potential range. The total faradaic efficiency values of up to 100% for glycerol oxidation catalyzed by MnO₂/CP suggest negligible contributions of any other redox process to the total current. Additionally, methane diol and formaldehyde can be detected by ¹³C NMR spectroscopy and phloroglucinol method (**Figure S24**), which are considered as the intermediate products during the bond breaking oxidation of glycerol in this work. In addition, the oxidation products of other alcohols such as ethylene glycol were also tested and analyzed as shown in **Figure S26-27**. In situ Transform Infrared (FTIR) spectroscopy was adopted to further shed light on the glycerol oxidation process (**Figure 3c**). The peak at ~1740 cm⁻¹ can be assigned to the formation of species containing a carbonyl group, such as aldehydes and carbonyl acids, which are hard to distinguish in the IR spectra because almost all products of glycerol oxidation contain a carbonyl group.^[16] The absorption bands at ~1240, and ~1364 and ~1385 cm⁻¹ are considered to belong to COOH.^[17] Besides, the asymmetric (O-C-O) stretching of COO* (~1541 and ~1519 cm⁻¹) is visible in this spectrum.^[18] According to analysis of in situ FTIR and ex situ NMR results, a possible pathway of glycerol oxidation catalyzed by MnO₂/CP under acid condition is proposed.^[19] As illustrated by **Figure S25**, formic acid generated by glycerol oxidation via the C-C bond cleavage may be further oxidized into carbon monoxide and carbon dioxide. In another path, formaldehyde formed by glycerol oxidation could be hydrated to form methane diol, which can either be directly oxidized to formic acid or re-adsorbed on the surface to form COO*, which can be further oxidized to carbon dioxide or carbon monoxide.

Mechanistic insight

RESEARCH ARTICLE

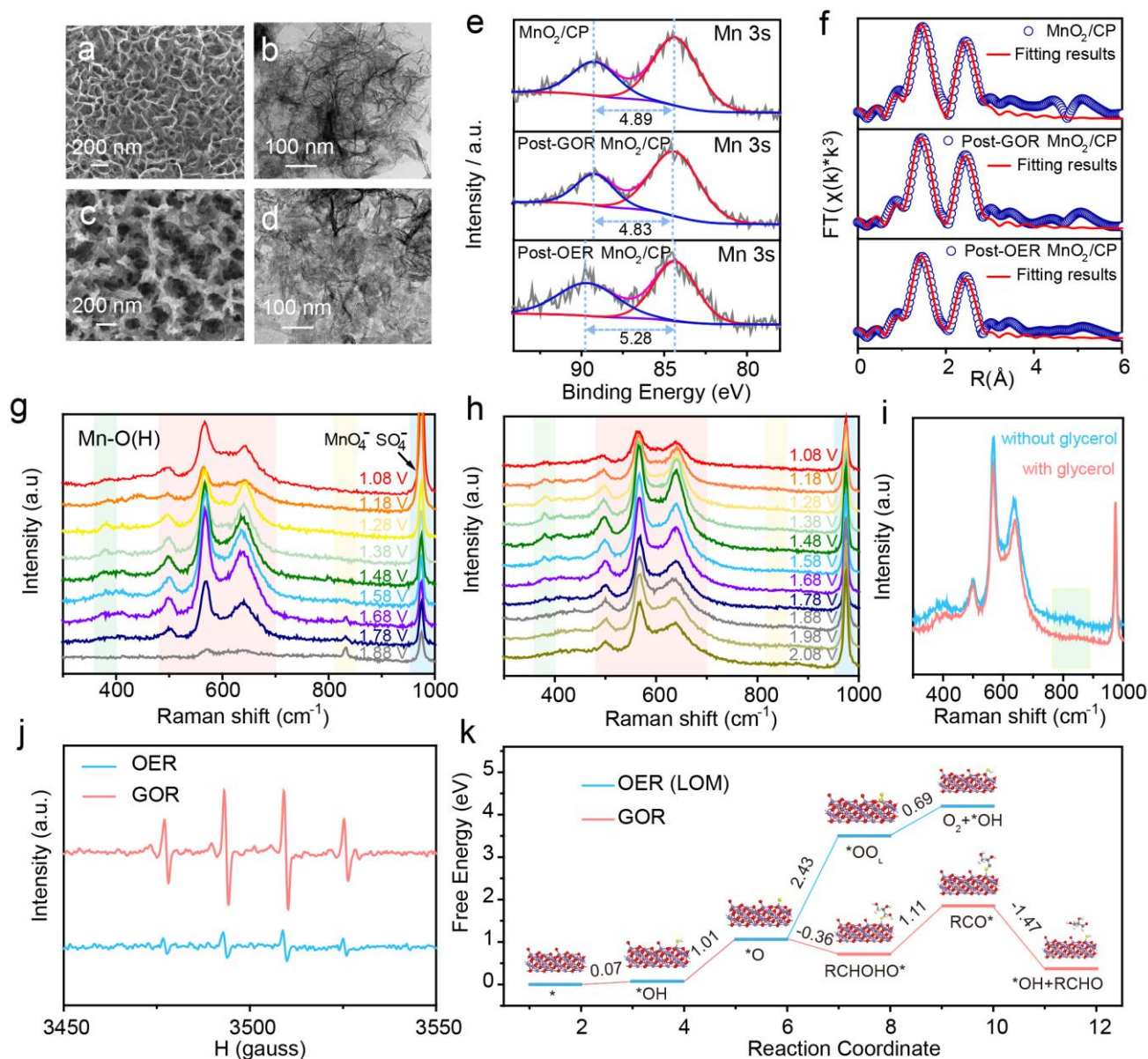


Figure 4 (a) SEM and (b) TEM images of the Post-GOR MnO₂/CP. (c) SEM and (d) TEM images of Post-OER MnO₂/CP. (e) Enlarged XPS spectra of Mn 3s of as-prepared MnO₂/CP, Post-GOR MnO₂/CP and Post-OER MnO₂/CP. (f) Fourier transforms of k^3 -weighted EXAFS experimental data of as-prepared MnO₂/CP, Post-GOR MnO₂/CP and Post-OER MnO₂/CP. Potential-dependent in situ Raman spectra of MnO₂/CP collected without (g) and with (h) the addition of glycerol. (i) in situ Raman spectra of MnO₂/CP collected with and without glycerol at applied potential of 1.58 V. (j) ESR detection of formed hydroxyl radicals in electrolyte during GOR and OER catalyzed by MnO₂/CP. (k) Reaction free-energy diagram of OER (LOM) and glycerol oxidation to glyceraldehyde

The remarkably differentiated activities and stabilities of the MnO₂/CP electrode catalyst for GOR and OER strongly suggest substantially different electro-catalytic pathways between the two processes. To reveal such a difference, we first quantified the dissolved Mn amounts during the GOR and OER by inductively coupled plasma optical emission spectrometry (ICP-OES). In 24 h of electrolysis at 10 mA cm⁻², the MnO₂/CP catalyst after GOR (Post-GOR MnO₂/CP) shows a ~4.80% weight loss of Mn relative to the fresh MnO₂/CP, which is markedly lower than that of ~10.48% of the MnO₂/CP catalyst after OER (Post-OER MnO₂/CP) (Figure S28a). Similar results can be obtained from the measurements of post-reaction catalysts operated at higher current densities (Figure S28b). Note that all these values are obviously lower than

the weight loss of MnO₂/CP in acidic electrolytes under same conditions without applying any potential (98.11%), implying the dissolution of the MnO₂ species at the positively charged anode can be largely suppressed under the anodic electrochemical conditions, as previously reported in literature.^[13a] The SEM and TEM images further reveal the different influences of these two operations on the morphology of MnO₂/CP electrode as presented in Figure 4a-d and Figure S29. Moreover, the Post-GOR MnO₂/CP remains its pristine γ -MnO₂ structure as evidenced by XRD patterns (Figure S30), comparatively, however, the XRD reflections of the Post-OER MnO₂/CP becomes weakened, implying the possible structural damage of MnO₂/CP during OER, which results in the poor stability.

RESEARCH ARTICLE

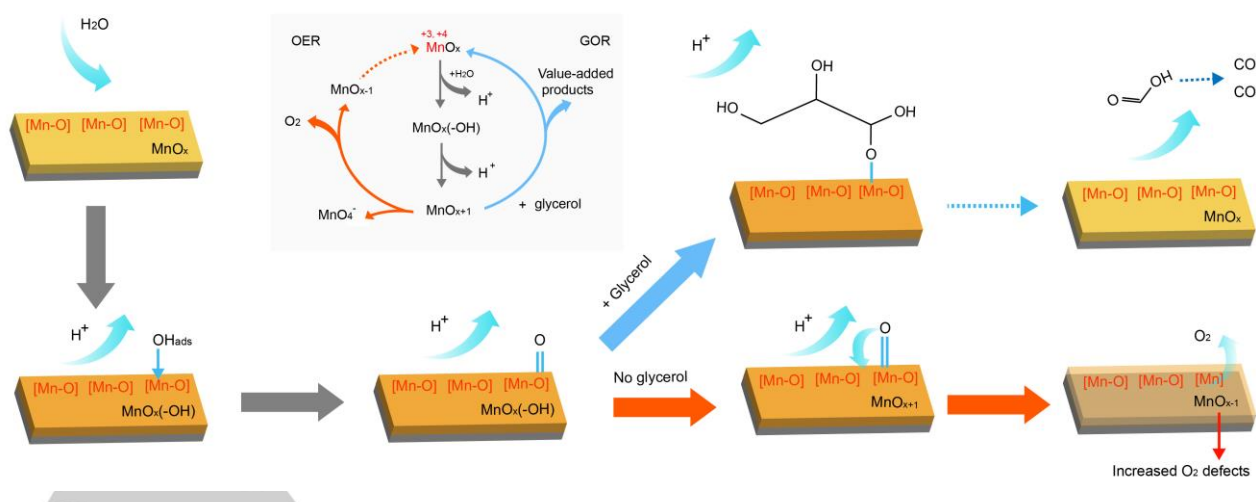
MnO₂/CP electrode before and after the GOR/OER operations have been characterized using ex situ XPS and X-ray absorption spectroscopy (XAS) measurements to understand the electronic changes occurring at the Mn and O centres during the reaction process under acid conditions. As exhibited in **Figure 4e** and **Table S5**, the peak energy separation (ΔE) between the two peaks in the high-resolution Mn XPS spectrum of Post-GOR MnO₂/CP decreases slightly from 4.89 to 4.83 eV, revealing a slightly increased valence state of Mn in the catalyst after GOR. In contrast, the ΔE value of Post-OER MnO₂/CP has been measured to increase to 5.28 eV, suggesting a much lowered valence state of the catalyst after OER, which is in accordance with the introduction of abundant oxygen defects in the catalyst as demonstrated by **Figure S31** and **Table S6**. The Mn K-edge X-ray adsorption near edge structure (XANES) spectra of Post-OER MnO₂/CP and Post-GOR MnO₂/CP (**Figure S32**) display negligible and significantly positive changes relative to their initial state, respectively, further confirming the above results.^[20] Further structural information was obtained by extended X-ray absorption fine structure (EXAFS) measurement to understand the configuration and local coordination environment (**Figure 4f**, **Figure S33** and **Table S7**).^[21] **Figure 4f** shows two peaks at around 1.89 Å and 2.85 Å in R-space spectra, which are originated from the Mn-O and Mn-Mn bonds, respectively. The fitting results show a larger oxygen coordination number (4.3) to Mn in Post-GOR MnO₂/CP and a smaller one (3.9) to Mn in Post-OER MnO₂/CP than that of the as-prepared MnO₂/CP, respectively, indicating an opposite change of oxygen defect concentration during these two reactions,^[20, 22] which agree well with the O 1s XPS data.

To further investigate the mechanism of GOR and OER over MnO₂/CP anode, in situ electrochemical Raman spectra were obtained in acidic solutions with and without the glycerol addition. **Figure 4g** displays the potential-dependent Raman spectral traces of MnO₂/CP catalyst for OER. According to a previous report, the bands in the region of about 490 - 700 cm⁻¹ can be interpreted as the stretching vibrations of MnO₆ octahedra and the sharp peak located at 975 cm⁻¹ corresponds to SO₄²⁻.^[23] Upon elevating the applied potential to 1.08 V vs. RHE, a strong peak

at 566 cm⁻¹ and a relatively weak peak 380 cm⁻¹ can be observed which can be attributed to the in-plane stretching vibrations of octahedral layers in MnO₂ and the terminal Mn-O(H) tunnel or surface stretches, respectively, implying the possible adsorption of water molecules. With the increase of applied potential up to 1.58 V, the peak at 833cm⁻¹ ascribed to the MnO₄⁻ species appears and further intensifies gradually at and above 1.68 V, which will de-stabilize the catalyst.^[24]

In situ Raman spectroscopic results obtained in the electrolyte with the addition of glycerol are shown in **Figure 4h**. Similarly, the species of Mn-O(H) can also be observed at 1.08 V. However, compared to that without the glycerol addition, no peak of MnO₄⁻ can be found at the increased potential applied, which is a clear evidence for the excellent stability of GOR. **Figure 4i** compares the results between with (GOR) and without (OER) glycerol at the potential of 1.58 V. A relatively strong spectral band at around 800 cm⁻¹ belonging to Mn-oxo (Mn^{IV}=O oxygen species)^[25] could be observed during OER. In the presence of glycerol, however, the peak intensity at around 800cm⁻¹ is significantly lower than that in the OER, and no signal belonging to MnO₄⁻ can be found, indicating the substantial protection effect of glycerol molecules against Mn^{IV}=O complex oxidation into MnO₄⁻ soluble in the electrolyte, and the resultant excellent durability of the MnO₂/CP catalyst.

According to experiment results and literature reports^[26], the possible mechanisms of GOR and OER catalyzed by MnO₂/CP catalysts under acidic conditions are proposed as shown in **Scheme 2**. It is well known that H₂O in electrolyte will be adsorbed on the metal oxides at anode and then lose electrons to form a hydroxyl radical-adsorbed species (MnO_x(-OH)) benefitting from the abundant d-orbitals of Mn element under the action of surface electric field. The adsorbed hydroxyl radicals will react with oxygen atoms in the lattice of manganese oxide to form MnO_{x+1} owing to the strong Mn-OH bonding.^[27] O₂ is then released from this chemical adsorbed "active oxygen" in MnO_{x+1}, which takes away one oxygen atom from the lattice. This process is considered as the lattice oxygen mechanism (LOM, a process usually taking place with metal dissolution and V_o formation and thus leading to catalyst structural damage), which, together with



Scheme 2. Schematics of the proposed mechanism for GOR and OER on MnO₂/CP catalysts in acid media

RESEARCH ARTICLE

the conventional adsorbate evolution mechanism, are considered to be the most accepted two routes for the structural instability during acidic OER.^[3a] In addition, the catalyst will dissolve as MnO_4^- (the species derived from the further $\text{Mn}^{\text{IV}}=\text{O}$ complex oxidation) in the electrolyte at the potential higher than 1.58 V. As a result, the electrocatalytic activity of MnO_2/CP catalyst will be substantially deteriorated during this OER process because of not only the significant decrease of Mn valence state and the noticeable increase of oxygen vacancy concentrations in the above experimental results, but also the further oxidation of $\text{Mn}^{\text{IV}}=\text{O}$ into soluble MnO_4^- species. Once added, glycerol molecule possessing stronger reducing potential than water is believed to be preferably anchored on the MnO_2 owing to its strong electron donation capability to the positively charged anodic catalyst during the electrolytic operation. Such anchored glycerol molecules can not only shield the catalyst against the dissolution by preferentially interacting with $\text{Mn}^{\text{IV}}=\text{O}$ to prevent its further oxidation into MnO_4^- , but more importantly, they can also prevent the formation of chemisorbed oxygen (an important step in producing oxygen leading to the destruction of the catalyst). As a result, the oxide catalyst is protected from deterioration via the glycerol adsorbing, while the adsorbed glycerol will be oxidized more favorably than water to form carbonaceous chemicals instead of oxygen by water oxidation, due to the stronger reductive potential of glycerol than water on the electrode. This pathway of preferred glycerol oxidation can be supported by the much higher concentration of hydroxyl radicals produced in post-GOR electrolyte than that in post-OER electrolyte observed by ESR (Figure 4j).^[2b]

Density functional theory (DFT) calculations were carried out to further support the above mechanisms. On the basis of the characterization results, the surface of the prepared catalyst was characterized by a MnO_2 (021) model. Since the oxidation of glycerol is a multi-step process, the calculation has been simplified to only account for the oxidation of glycerol to glyceraldehyde to compare with the OER process via LOM. As shown in Figure 4k, the reaction branches after the formation of $^*\text{O}$ intermediate, and the energy barrier to form $^*\text{OO}_\text{L}$ ($\Delta G = 2.43$ eV) is significantly higher than that for RCHOHO^* ($\Delta G = -0.36$ eV). The DFT results demonstrate that in the presence of RCH_2OH ($\text{R}=\text{CH}_2\text{OHCHOH}$), the produced $^*\text{O}$ intermediate will react with the RCH_2OH to produce RCHO instead of coupling with lattice oxygen to produce O_2 , in consistency with the experimental results. Collectively, in acidic aqueous solutions without the addition of glycerol, besides the dissolution of the MnO_2 by forming MnO_4^- soluble in electrolyte, lattice structure of catalyst will become gradually collapsed due to the high concentration of oxygen vacancies created in the MnO_2 lattice; while the introduction of reductive glycerol can protect the catalyst from deactivation by inhibiting both LOM and the $\text{Mn}^{\text{IV}}=\text{O}$ oxidation into MnO_4^- , thus favouring the long-term stability of the MnO_2/CP at anode in electrocatalytic hydrogen production system.

Conclusion

In summary, non-precious metal MnO_2/CP electrocatalyst in coordination with alcohol oxidation demonstrate not only significantly decreased total energy input for hydrogen production, but also unexpected but most favorable ultra-long durability in acidic electrolytes. Especially, the electrocatalytic oxidations of

alcohols possessing hydroxyl groups on adjacent carbon show significantly reduced anodic potential and excellent stability compared with traditional electrocatalytic water splitting. In particular, the electrocatalytic glycerol oxidation in coupling with water reduction not only enables the efficient productions of hydrogen and value-added formic acid instead of oxygen, but can also be operated at an especially low potential (1.36 V vs. RHE) for more than 865 hours, which is greatly longer than that in the absence of glycerol. The presence of alcohol molecules, such as glycerol, has been proposed to protect the catalyst from degradation by stabilizing the manganese valence and diminishing the excessive oxygen vacancies, therefore favoring the ultra-long stability of MnO_2/CP . The in situ Raman spectroscopic analysis and DFT calculation further manifest the effect of glycerol addition on enhancing the stability of MnO_2 via the inhibitions of both lattice oxygen process and MnO_2 dissolution. Such a finding may open an unprecedented window in searching novel non-noble metal catalysts for applications in electrochemical hydrogen and value-added chemical productions by alcohol oxidation under acidic conditions.

Supporting Information

Supporting Information is available from the Wiley Online Library or from the author.

Acknowledgements

This work was supported by Natural Science Foundation of Shanghai (21ZR1418700), China Postdoctoral Science Foundation funded project (2020T130193). The authors would like to thank ECNU Multifunctional Platform for Innovation for support of SEM and TEM characterizations (004). The authors thank beamline BL14W1 (Shanghai Synchrotron Radiation Facility) for providing the beam time. We gratefully acknowledge Dr. Yuan Yuan at the East China Normal University for his help with the Raman analysis.

Keywords: acidic electrolyte • non-noble metal • manganese oxide catalyst • glycerol oxidation reaction • electrocatalytic hydrogen production

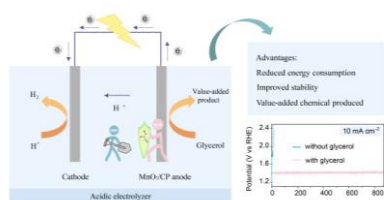
- [1] a) M. Blasco-Ahicart, J. Soriano-López, J. J. Carbo, J. M. Poblet, J. R. Galan-Mascaros, *Nat. Chem.* **2017**, *10*, 24-30.; b) H. Xu, H. Shang, C. Wang, Y. Du, *Coord. Chem. Rev.* **2020**, *418*, 213374.
- [2] a) H. Xu, H. Shang, L. Jin, C. Chen, C. Wang, Y. Du, *J. Mater. Chem. A* **2019**, *7*, 26905-26910; b) H. Xu, H. Shang, C. Wang, L. Jin, C. Chen, C. Wang, Y. Du, *Appl. Catal. B* **2020**, *265*, 118605.
- [3] a) L. An, C. Wei, M. Lu, H. Liu, Y. Chen, G. G. Scherer, A. C. Fisher, P. Xi, Z. J. Xu, C. H. Yan, *Adv. Mater.* **2021**, *33*, e2006328; b) M. Carmo, D. L. Fritz, J. Mergel, D. Stolten, *Int. J. Hydrogen Energy* **2013**, *38*, 4901-4934.
- [4] a) P. Li, R. Zhao, H. Chen, H. Wang, P. Wei, H. Huang, Q. Liu, T. Li, X. Shi, Y. Zhang, M. Liu, X. Sun, *Small* **2019**, *15*, 1805103; b) Y. Li, X. Wei, L. Chen, J. Shi, *Angew. Chem. Int. Ed.* **2021**, *60*, 2-24.; c) G. Wu, X. Zheng, P. Cui, H. Jiang, X. Wang, Y. Qu, W. Chen, Y. Lin, H. Li, X. Han, Y. Hu, P. Liu, Q. Zhang, J. Ge, Y. Yao, R. Sun, Y. Wu, L. Gu, X. Hong, Y. Li, *Nat. Commun.* **2019**, *10*, 4855; d) M. Chatti, J. L. Gardiner, M. Fournier, B. Johannessen, T. Williams, T.

RESEARCH ARTICLE

- R. Gengenbach, N. Pai, C. Nguyen, D. R. MacFarlane, R. K. Hocking, A. N. Simonov, *Nat. Catal.* **2019**, *2*, 457-465.
- [5] B. You, X. Liu, N. Jiang, Y. Sun, *J. Am. Chem. Soc.* **2016**, *138*, 13639-13646.
- [6] a) X. Wei, S. Wang, Z. Hua, L. Chen, J. Shi, *ACS Appl. Mater. Interfaces* **2018**, *10*, 25422-25428; b) Y. Huang, X. Chong, C. Liu, Y. Liang, B. Zhang, *Angew. Chem. Int. Ed.* **2018**, *57*, 13163; c) Y. Li, X. Wei, L. Chen, J. Shi, M. He, *Nat. Commun.* **2019**, *10*, 5335.
- [7] a) M. Huynh, C. Shi, S. J. L. Billinge, D. G. Nocera, *J. Am. Chem. Soc.* **2015**, *137*, 14887-14904; b) Y. Tang, S. Zheng, S. Cao, H. Xue, H. Pang, *J. Mater. Chem. A* **2020**, *8*, 18492-18514; c) H. Wang, F. Yin, B. Chen, G. Li, *J. Mater. Chem. A* **2015**, *3*, 16168-16176; d) A. Li, H. Ooka, N. Bonnet, T. Hayashi, Y. Sun, Q. Jiang, C. Li, H. Han, R. Nakamura, *Angew. Chem. Int. Ed.* **2019**, *58*, 5054-5058; e) R. Frydendal, E. A. Paoli, I. Chorkendorff, J. Rossmeisl, I. E. L. Stephens, *Adv. Energy Mater.* **2015**, *5*, 1500991.
- [8] a) C. Y. and J. Parmentier, et al., *Progress in Solid State Chemistry* **1995**, *23*, 1-130; b) S. Chou, F. Cheng, J. Chen, *J. Power Sources* **2006**, *162*, 727-734.
- [9] a) M. C. a. M. Ishikawa, *J. Electrochem. Soc.* **2000**, *147*, 2246-2251; b) Mathieu Toupin, *Chem. Mater.* **2002**, *14*, 3946-3952; c) Cerrato, J. M., Hochella, M. F., Knocke, W. R., Dietrich, A. M. & Cromer, T. F; *Environ. Sci. Technol.* **2010**, *44*, 5881-5886; d) P. Gao, P. Metz, T. Hey, Y. Gong, D. Liu, D. D. Edwards, J. Y. Howe, R. Huang, S. T. Mixture, *Nat. Commun.* **2017**, *8*, 14559.
- [10] a) H. Tian, L. Zeng, Y. Huang, Z. Ma, G. Meng, L. Peng, C. Chen, X. Cui, J. Shi, *Nano-Micro Lett.* **2020**, *12*, 161; b) S. Gao, Z. Sun, W. Liu, X. Jiao, X. Zu, Q. Hu, Y. Sun, T. Yao, W. Zhang, S. Wei, Y. Xie, *Nat. Commun.* **2017**, *8*, 14503.
- [11] K. Xiang, D. Wu, X. Deng, M. Li, S. Chen, P. Hao, X. Guo, J. L. Luo, X. Z. Fu, *Adv. Funct. Mater.* **2020**, *30*, 1909610.
- [12] N. Li, T. P. Keane, S. S. Veroneau, R. G. Hadt, D. Hadt, L. X. Chen, D. G. Nocera, *PNAS* **2020**, *117*, 16187-16192.
- [13] a) M. Huynh, D. K. Bediako, D. G. Nocera, *J. Am. Chem. Soc.* **2014**, *136*, 6002-6010; b) D. K. Bediako, C. C. Costentin, E. C. Jones, D. G. Nocera, J. Savéant, *J. Am. Chem. Soc.* **2013**, *135*, 10492-10502.
- [14] A. Wu, Y. Xie, H. Ma, C. Tian, Y. Gu, H. Yan, X. Zhang, G. Yang, H. Fu, *Nano Energy* **2018**, *44*, 353-363.
- [15] a) Liang, S., Teng, F., Bulgan, G., Zong, R. Zhu, Y., *J. Phys. Chem. C* **112**, 5307-5315; b) E. Hayashi, Y. Yamaguchi, K. Kamata, N. Tsunoda, Y. Kumagai, F. Oba, M. Hara, *J. Am. Chem. Soc.* **2019**, *141*, 890-900; c) W. Wei, X. Cui, W. Chen, D. G. Ivey, *J. Power Sources* **2009**, *186*, 543-550.
- [16] L. Huang, Y. Sun, H. Cao, M. Zhan, R. Ni, J. Sun, Z. Chen, Y. Zhou, E. G. Sorte, J. Tong, G. Sun, *ACS Catal.* **2016**, *6*, 7686-7695.
- [17] M. S. E. Houache, R. Safari, U. O. Nwabara, T. Rafaideen, G. A. Botton, P. J. A. Kenis, S. Baranton, C. Coutanceau, E. A. Baranova, *ACS Appl. Energy Mater.* **2020**, *3*, 8725-8738.
- [18] N. J. Firet, W. A. Smith, *ACS Catal.* **2016**, *7*, 606-612.
- [19] a) Y. Kwon, Y. Birdja, I. Spanos, P. Rodriguez, M. T. M. Koper, *ACS Catal.* **2012**, *2*, 759-764; b) P. Pullanikat, J. H. Lee, K. S. Yoo, K. W. Jung, *Tetrahedron Lett.* **2013**, *54*, 4463-4466; c) Y. Zhao, C. Chang, F. Teng, Y. Zhao, G. Chen, R. Shi, G. I. N. Waterhouse, W. Huang, T. Zhang, *Adv. Energy Mater.* **2017**, *7*, 1700005.
- [21] S. Lian, M. P. Browne, C. Domínguez, S. N. Stamatina, H. Nolan, G. S. Duesberg, M. E. G. Lyons, E. Fonda, P. E. Colavita, *Sustain. Energ. Fuels* **2017**, *1*, 780-788.
- [22] X. Li, J. Ma, L. Yang, G. He, C. Zhang, R. Zhang, H. He, *Environ. Sci. Technol.* **2018**, *52*, 12685-12696.
- [23] D. Chen, D. Ding, X. Li, G. H. Waller, X. Xiong, M. A. El-Sayed, M. Liu, *Chem. Mater.* **2015**, *27*, 6608-6619.
- [24] a) K. H. Cho, S. Park, H. Seo, S. Choi, M. Y. Lee, C. Ko, K. T. Nam, *Angew. Chem. Int. Ed.* **2021**, *60*, 4673; b) W. Kiefer, H. J. Bernstein, *Mol. Phys.* **2006**, *23*, 835-851.
- [25] a) S. C. Sawant, X. Wu, J. Cho, K. B. Cho, S. H. Kim, M. S. Seo, Y. M. Lee, M. Kubo, T. Ogura, S. Shaik, W. Nam, *Angew. Chem. Int. Ed.* **2010**, *49*, 8190-8194; b) R. S. Czernuszewicz, Y. O. Su, M. K. Stern, K. A. Macor, D. Kim, J. T. Groves, and T. G. Spiro, *J. Am. Chem. Soc.* **1988** *110* (13), 4158-4165.
- [26] K. Jin, H. Seo, T. Hayashi, M. Balamurugan, D. Jeong, Y. K. Go, J. S. Hong, K. H. Cho, H. Kakizaki, N. Bonnet-Mercier, M. G. Kim, S. H. Kim, R. Nakamura, K. T. Nam, *J. Am. Chem. Soc.* **2017**, *139*, 2277-2285.
- [27] R. Subbaraman, D. Tripkovic, K. C. Chang, D. Strmcnik, A. P. Paulikas, P. Hirunsit, M. Chan, J. Greeley, V. Stamenkovic, N. M. Markovic, *Nat. Mater.* **2012**, *11*, 550-557.
- [28] G. Chen, *Sep. Pur. Technol.* **2004**, *38*, 11-41.

RESEARCH ARTICLE

Entry for the Table of Contents



This work reports a strategy of using low-cost acidic aqueous solution of alcohols for efficient hydrogen/chemical co-production. The as-prepared non-precious metal MnO_2/CP electrocatalyst in coordination with alcohol oxidation demonstrate not only significantly decreased total energy input for hydrogen production, but also ultra-high durability in acidic electrolytes.